JACS
JOURNAL OF THE AMERICAN CHEMICAL SOCIETY
Article
pubs.acs.org/JACS

Reversible Intermolecular E−H Oxidative Addition to a Geometrically Deformed and Structurally Dynamic Phosphorous Triamide

Wei Zhao,[†] Sean M. McCarthy,[†] Ting Yi Lai,[†] Hemant P. Yennawar,[†,‡] and Alexander T. Radosevich*[,†]

[†]Department of Chemistry and [‡]X-ray Crystallography Laboratory, Department of Biochemistry and Molecular Biology, The Pennsylvania State University, University Park, Pennsylvania 16802, United States

Supporting Information

ABSTRACT: The synthesis and reactivity of geometrically constrained tricoordinate phosphorus (σ^3-P) compounds supported by tridentate triamide chelates ($N[o\text{-}NR\text{-}C_6H_4]_2^{3-}$; R = Me or ^{i}Pr) are reported. Studies indicate that **2** ($P\{N[o\text{-}NMe\text{-}C_6H_4]_2\}$) adopts a C_s-symmetric structure in the solid state. Variable-temperature NMR studies demonstrate a low-energy inversion at phosphorus in solution ($\Delta G^{\ddagger}_{exptl}{}^{298}$ = 10.7(5) kcal/mol), for which DFT calculations implicate an edge-inversion mechanism via a metastable C_2-symmetric intermediate. In terms of reactivity, compound **2** exhibits poor nucleophilicity, but undergoes oxidative addition at ambient temperature of diverse O−H- and N−H-containing compounds (including alcohols, phenols, carboxylic acids, amines, and anilines). The resulting pentacoordinate adducts **2**·[H][OR] and **2**·[H][NHR] are characterized by multinuclear NMR spectroscopy and X-ray crystallography, and their structures (which span the pseudorotation coordinate between trigonal bipyramidal and square planar) are evaluated in terms of negative hyperconjugation. At elevated temperatures, the oxidative addition is shown to be reversible for volatile alcohols and amines.

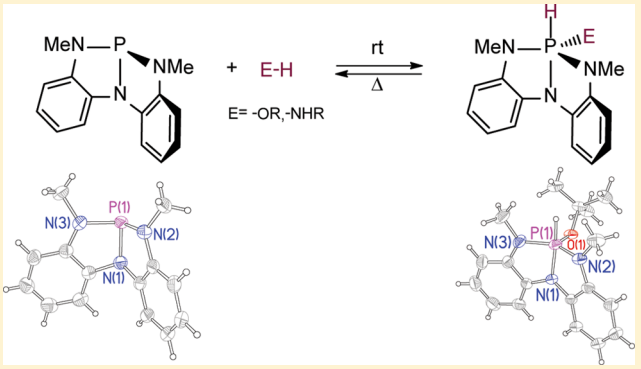

1. INTRODUCTION

Neutral tricoordinate phosphorus (σ^3-P) compounds commonly exhibit pyramidal structures with local 3-fold (C_{3v}) symmetry about phosphorus.[1] The electronic structure imbued by this geometry is associated with a filled frontier lone pair that is sterically and electronically accessible to electron-deficient reactants.[2] The Lewis basicity and nucleophilicity of σ^3-P compounds that emanate from this common understanding underpin essentially all of their applications in modern synthesis,[3] coordination chemistry,[4] and catalysis.[5]

Molecular distortions of the σ^3-P framework within 3-fold symmetry have been the focus of extensive experimental and theoretical investigation. Displacement along the umbrella inversion coordinate is associated with a second-order Jahn−Teller effect that stabilizes the C_{3v} pyramidal structure.[6,7] The energetic barrier to dynamic interconversion of ground-state C_{3v} structures via a D_{3h} transition state is on the order of 25−40 kcal/mol for typical trivalent aryl- and alkylphosphorus compounds.[8] Flattening of the ground-state phosphorus pyramid has been achieved through a variety of steric and electronic effects,[9] and these lead to a commensurate lowering of the inversion barrier.[10]

There are, by contrast, fewer examples of σ^3-P compounds that deviate significantly from local 3-fold symmetry. Most notable in this class are the unusual C_{2v} symmetric σ^3-P compounds (e.g., **1**, Figure 1) prepared and investigated by

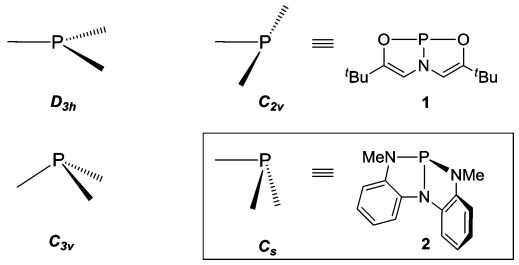

Figure 1. Molecular shapes of tricoordinate phosphorus compounds.

Arduengo.[11,12] Remarkably, the fused heterobicyclic core that contains the tricoordinate phosphorus is molecularly flat, with the tridentate *O,N,O*-binding motif occupying three adjacent coplanar sites. As in related delocalized heterocyclic systems,[13] the T-shaped geometry is stabilized by extensive resonance in the π-plane of the molecule.[14]

We have been interested in the chemistry of distorted tricoordinate phosphorus as a potential nonmetal platform for bond activation and catalysis.[15] In this regard, we have demonstrated that **1** undergoes reaction to give phosphorane (σ^5-P) products by small-molecule bond activation and that this σ^3-P ⇌ σ^5-P interconversion can be leveraged for catalysis.[16,17]

Received: October 14, 2014
Published: November 17, 2014

   dx.doi.org/10.1021/ja510558d | J. Am. Chem. Soc. 2014, 136, 17634−17644

We have further shown that the severe geometric distortion of **1** imparts significant electrophilic character at phosphorus as opposed to the typical Lewis basicity of σ^3-P compounds.

In an effort to ascertain the extent to which alternative deviations from 3-fold symmetry about phosphorus might impart noncanonical reactivity,[18] we were drawn to consider the chemistry of phosphorous triamides (i.e., compounds containing the PN_3 core). Specifically, Mitzel et al. have shown,[19] in accord with earlier spectroscopic studies,[20] that $P(NMe_2)_3$ is inherently nontrigonal, adopting molecular C_s symmetry as determined by X-ray crystallography. The distortion away from 3-fold symmetry in this case, however, is modest; the difference in bond angles about phosphorus ($\Delta\angle N_x{-}P{-}N_y$) is only ca. 13°, and the computed energy difference (MP2/6-31G*) between the C_s and C_3 structures is just 6.8 kcal/mol. Consequently, $P(NMe_2)_3$ behaves chemically much as would be expected for a σ^3-P compound with typical pyramidal geometry, exhibiting potent Lewis basicity and nucleophilicity.[21]

In this paper, we describe the synthesis and reactivity of a chelated σ^3-P phosphorous triamide (**2**) with an exaggerated C_s distortion. We demonstrate the extent to which this distortion impacts the ground-state electronic structure of **2**, and we document solution-phase conformational dynamism involving low-energy inversion at phosphorus. With respect to reactivity, we show that the molecular deformation toward C_s symmetry enforced by the chelate greatly diminishes the nucleophilicity of the phosphorus center, but renders it reactive with respect to reversible intermolecular oxidative addition of both O–H and N–H compounds under mild conditions. In sum, these results show that the imposition of low symmetry at tricoordinate phosphorus leads to electronic structures and reactivity of the type that might be desirable for novel reaction design.

2. RESULTS

2.1. Synthesis and Characterization of 2. *2.1.1. Preparation and Spectroscopy.* The triamine **3a** was prepared in three steps on a multigram scale according to the procedure of Hu.[22] Insertion of phosphorus(III) into this chelate by treatment with PCl_3 and triethylamine in a mixed THF/Et_2O solvent proceeded cleanly with elimination of triethylammonium chloride to give target phosphorous triamide **2** in 80% yield as an off-white solid (eq 1). An *N*-isopropyl analogue (**4**) was prepared in similar fashion from **3b** in 83% yield.

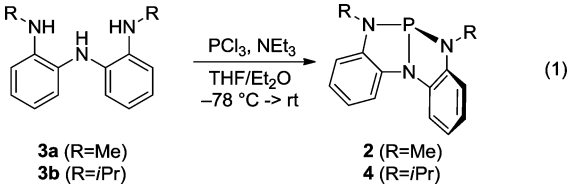

3a (R=Me)
3b (R=*i*Pr)

2 (R=Me)
4 (R=*i*Pr)

(1)

For compound **2**, a $^{31}P\{^1H\}$ NMR spectrum confirms the formation of a single phosphorus containing product with a chemical shift δ 159.8 ppm. The ^1H NMR spectrum shows a single resonance for the *N*-methyl substituents (δ 3.12 ppm) which is split into a doublet (J = 8.4 Hz) as a function of ^3J coupling to the phosphorus center. The eight aryl hydrogens give rise to four resonances between δ 7.50 ppm and δ 6.66 ppm, indicative of a molecular symmetry that renders the two aryl moieties equivalent. Compound **2** is stable indefinitely under inert atmosphere both in the solid state and in solution; however, upon exposure to air it undergoes slow decomposition via brightly colored burgundy intermediates, suggestive of initial oxidation of the triamide chelate as is well-known for this electron-rich fragment.[23]

2.1.2. Geometric and Electronic Structure. Concentration of a cooled pentane solution of **2** resulted in deposition of a microcrystalline solid suitable for X-ray diffraction. The solid-state structure of **2** (Figure 2) deviates strongly from the local

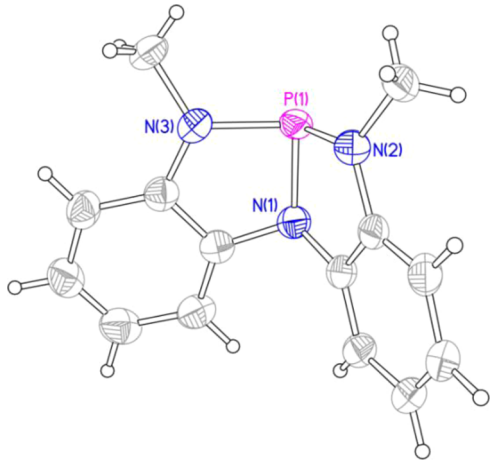

Figure 2. Thermal ellipsoid plot rendered at the 50% probability level for **2**.

C_{3v} symmetry that is common to trigonal pyramidal tricoordinate phosphorus compounds. Instead, the tridentate triamide motif enforces a strained geometry about phosphorus in **2** with significant folding along the $P_1{-}N_1$ axis, resulting in an essentially C_s-symmetric structure. Specifically, the two angles formed by proximal ligand nitrogen atoms with phosphorus are small and nearly equivalent ($\angle N_1{-}P{-}N_2$ = 90.51(6)°, $\angle N_1{-}P{-}N_3$ = 90.08(6)°); by contrast, the remaining angle between the remote ligand nitrogen atoms and phosphorus is significantly broader ($\angle N_2{-}P{-}N_3$ = 115.21(7)°). In effect, with these metrics the local structure around phosphorus approximates a *cis*-divacant trigonal bipyramid in which the triamide occupies one axial and two equatorial sites. Consistent with this notion, the bond distances from phosphorus to the pseudoequatorial *N*-methylanilide nitrogen atoms are nearly equivalent ($d(P_1{-}N_2)$ = 1.7014(14) Å, $d(P_1{-}N_3)$ = 1.7190(13) Å), whereas that to the pseudoaxial diarylamide nitrogen is significantly longer ($d(P_1{-}N_1)$ = 1.7610(12) Å).

The DFT-optimized structure of **2** (B3LYP/6-311+G**) corresponds closely to the crystallographic determination (Table 1), where the molecular geometry about the phosphorus atom resembles a distorted AX_3E electronic structure with a stereochemically active lone pair of electrons. According to natural bond orbital (NBO) analysis,[24] the phosphorus-based lone pair in this strained geometry resides in an s-rich nonbonding orbital of formal $sp^{0.54}$ hybridization (65% s-orbital character). Congruent with the high s-character of the lone pair, compound **2** is very poorly nucleophilic; it is not alkylated by benzyl bromide even after being refluxed in toluene for 12 h. Moreover, the corresponding terminal phosphine selenide **2**·[Se][25] displays a large $^1J_{^{31}P-^{77}Se}$ coupling constant (J = 907 Hz), a further indication of the high s-character on the lone pair at phosphorus.[26] For comparison, the related phosphorous triamide $(Me_2N)_3P$ is rapidly alkylated by benzyl bromide at

dx.doi.org/10.1021/ja510558d | J. Am. Chem. Soc. 2014, 136, 17634–17644

Table 1. Tabulated Bond Distances (Å) and Angles (deg) for 2 (Experimental and Computational), 2·[Se], $(Me_2N)_3P$, and $(Me_2N)_3P$·[Se][a]

	2				
metric	exptl	computed[b]	$(Me_2N)_3P$[c]	2·[Se]	$(Me_2N)_3P$·[Se][d]
$d(P_1-N_1)$	1.7610(12)	1.782	1.732(3)	1.699(3)	1.678(3)
$d(P_1-N_2)$	1.7014(14)	1.749	1.681(3)	1.677(3)	1.649(3)
$d(P_1-N_3)$	1.7190(13)	1.749	1.684(3)	1.667(3)	1.650(3)
$d(P_1-Se_1)$				2.0718(11)	2.114(1)
$\angle N_1-P_1-N_2$	90.51(6)	89.1	97.3(2)	93.81(14)	101.5(1)
$\angle N_1-P_1-N_3$	90.08(6)	89.1	97.5(2)	93.47(14)	107.3(1)
$\angle N_2-P_1-N_3$	115.21(7)	116.8	111.3(2)	116.60(14)	109.3(1)

[a]See the Supporting Information for full crystallographic details. [b]Structure optimized with B3LYP/6-311+G**. [c]Data from ref 19. Metrics for only one of two independent molecules in the asymmetric unit are tabulated here. [d]Data from ref 29.

room temperature[27] and exhibits a more modest $^1J_{^{31}P-^{77}Se}$ = 784 Hz for the corresponding terminal selenide $(Me_2N)_3P$·[Se].[28,29]

2.1.3. Dynamic Solution Behavior. Contrary to expectation for the C_s-symmetric structure determined for **2** in the solid state, the diastereotopic methyl groups of the *N*-isopropyl substituents of **4** appear as one doublet resonance (δ 1.51 ppm, J = 6.8 Hz) in an ambient-temperature ^{1}H NMR spectrum (300 MHz, THF-d_8). By contrast, two partially resolved doublets ($\Delta\nu$ = 30 Hz) are observed at −80 °C, with a signal coalescence temperature (T_c) of ca. −60 °C (Figure 3). Over the entire temperature range examined (25 °C > T > −80 °C), the ^{31}P chemical shift of **4** remains constant (δ 151.6 ppm). Taken together, this spectroscopic behavior indicates that a dynamic conformational process is responsible for rendering the diastereotopic methyl groups of **4** equivalent at ambient temperature. The rate constants for this process were estimated by line shape simulation of ^{1}H NMR spectra obtained over the temperature range of −35 °C > T > −80 °C (Figure 3). An approximate free energy of activation $\Delta G^{\ddagger}_{exptl}{}^{298}$ = 10.7(5) kcal/mol was estimated from the resulting Eyring plot (see the Supporting Information for full details). The small activation entropy thus derived [$\Delta S^{\ddagger}_{exptl}$ = −1(2) cal/(mol·K)] militates in favor of a unimolecular isomerization.

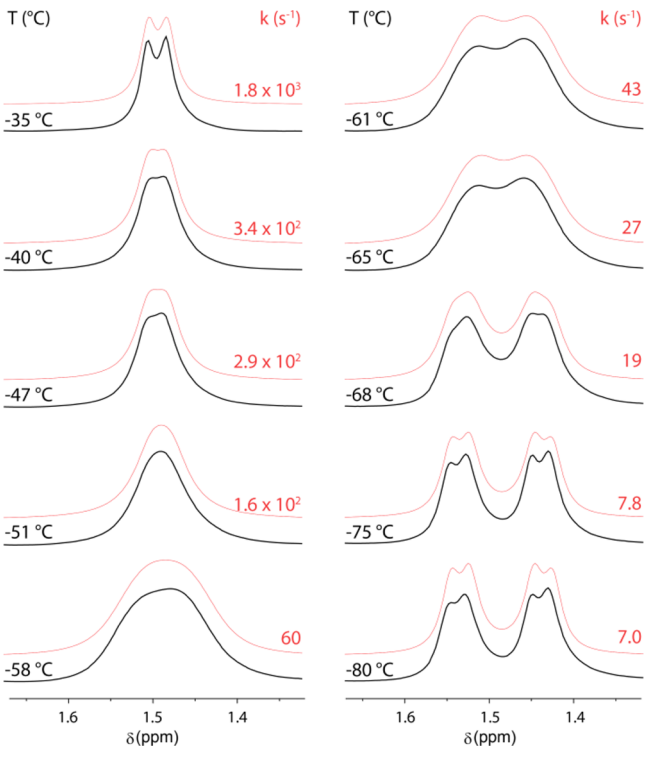

Figure 3. Variable-temperature ^{1}H NMR spectra of **4** illustrating the decoalescence of the diastereotopic methyl moieties below −60 °C. Experimental spectra in black, simulated spectra in red. See the Supporting Information for fitting parameters and Eyring analysis.

DFT calculations (B3LYP/6-311+G**) support the experimentally observed dynamic behavior and implicate a stepwise edge-inversion pathway at phosphorus.[30] Whereas the global minimum structure for **2** is computed to be C_s-symmetric as noted above, a stable C_2-symmetric conformer with local T-shaped geometry at phosphorus (Figure 4, bottom) can be identified as a minimum at only modestly increased energy (ΔG = +4.4 kcal/mol). These two conformers are connected on the potential energy surface by a C_1-symmetric transition structure with a computed free energy of $\Delta G^{\ddagger}$ = +5.7 kcal/mol relative to **2**. The exceptionally low barrier computed for inversion at phosphorus via this mechanism is in good agreement with the dynamic solution behavior determined by variable-temperature NMR (VT-NMR) spectroscopy.

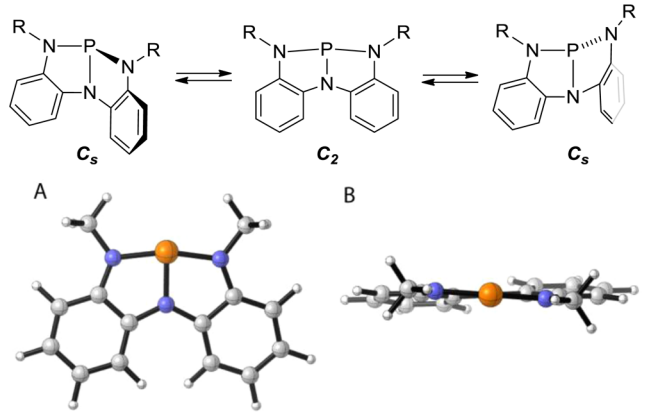

Figure 4. (Top) Proposed mechanism for the observed dynamic conformation of **2**/**4**. (Bottom) Computed C_2-symmetric T-shaped conformer of **2** (B3LYP/6-311+G**): (A) top view; (B) view down the C_2 axis.

A further indication of the extreme conformational flexibility of the *N*,*N*,*N*-chelate **3** about phosphorus is evident in the structure of the related dichlorophosphorane **2**·$[Cl]_2$, prepared in 74% isolated yield by treatment of triamine **3a** with

dx.doi.org/10.1021/ja510558d | J. Am. Chem. Soc. 2014, 136, 17634−17644

phosphorus pentachloride and triethylamine in dichloromethane (eq 2).

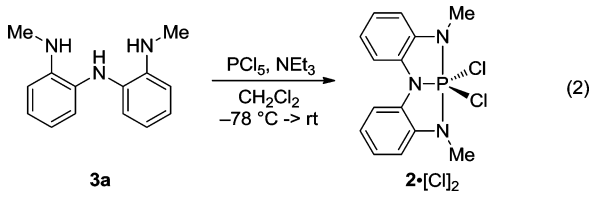

3a 2·[Cl]$_2$ (2)

As shown in Figure 5, the *N,N,N*-coordinating motif here adopts a meridional chelating mode in which the *N*-

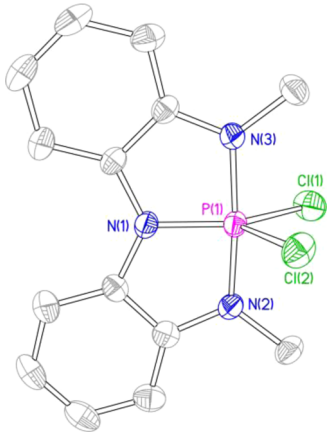

Figure 5. Thermal ellipsoid plot of 2·[Cl]$_2$ rendered at the 50% probability level. All hydrogens omitted for clarity. Selected bond distances (Å) and angles (deg): $d(P_1–N_1)$ = 1.7095(16); $d(P_1–N_2)$ = 1.7129(17); $d(P_1–N_3)$ = 1.7082(16); $d(P_1–Cl_1)$ = 2.1334(8); $\angle N_1–P_1–N_2$ = 87.73(8); $\angle N_1–P_1–N_3$ = 87.90(8); $\angle N_2–P_1–N_3$ = 172.22(8); $\angle N_1–P_1–Cl_1$ = 118.08(6); $\angle N_1–P_1–Cl_2$ = 139.02(6); $\angle Cl_1–P_1–Cl_2$ = 102.90(4).

methylanilide groups span apical positions of a phosphorus-centered trigonal bipyramid ($\angle N_2–P_1–N_3$ = 172.22(8)°) with the equatorial plane defined by the diarylamide nitrogen and two chloride ligands ($\Sigma\angle X_{eq}–P_1–Y_{eq}$ = 360°).

In summary, the collected data show triamine **3** to be a conformationally dynamic chelate capable of supporting diverse phosphorus compounds of various oxidation states by adopting distinct coordinating geometries.

2.2. Intermolecular E–H Oxidative Addition Reactivity of 2. *2.2.1. Oxidative Addition of O–H Compounds.* Although compound **2** is sparingly reactive with respect to common alkylating reagents (vide supra), it undergoes rapid intermolecular reaction with a range of protic reagents E–H.[31] For instance, treatment of **2** with a stoichiometric amount of dry ethanol at room temperature in chloroform led to rapid and quantitative consumption of **2**. Removal of volatiles gave a white solid for which a single new phosphorus resonance was identified in the ^{31}P NMR region characteristic of pentacoordinate compounds (δ −25.6 ppm, 145.78 MHz, $CDCl_3$). This resonance displays as a proton-coupled doublet ($^1J_{P–H}$ = 602 Hz) upon which longer range coupling can be discerned (apparent heptet, $^3J_{P–H}$ = 17 Hz). Complementary coupling is evident in the ^{1}H NMR spectra (300 MHz, $CDCl_3$); a broad doublet centered at δ 6.30 ppm ($^1J_{P–H}$ = 602 Hz) is assigned to a phosphorus-bound hydrogen substituent, and the ligand *N*-methyl groups (δ 3.15 ppm) present as a doublet ($^3J_{P–H}$ = 17 Hz). The combined multinuclear spectral data are therefore consistent with the formation of a stable phosphorane, **2**·[H][OEt], from O–H oxidative addition of ethanol to **2**, an assignment further corroborated by subsequent X-ray diffraction studies (vide infra).

Related primary (benzyl alcohol), secondary (cyclohexanol), and tertiary (*tert*-butyl alcohol) aliphatic alcohols are also found to undergo O–H oxidative addition to give adducts **2**·[H][OR] following removal of volatiles (Figure 6), and this reactivity

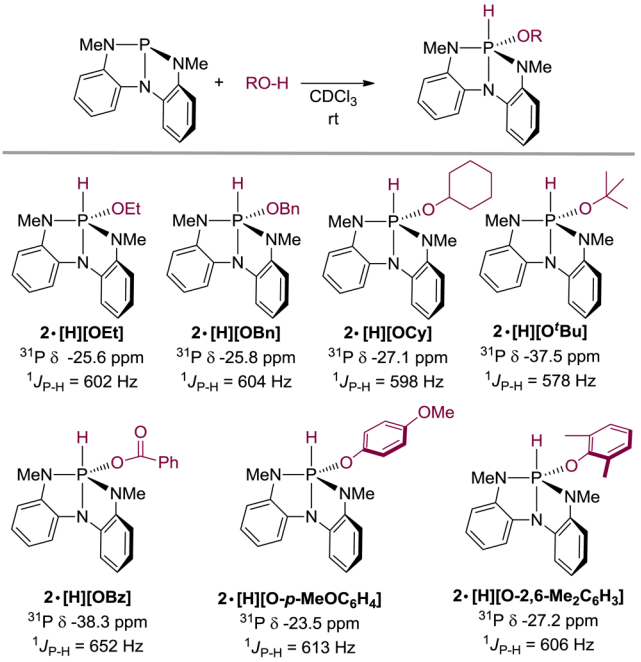

Figure 6. Examples of O–H oxidative addition to **2**, including key ^{31}P NMR parameters.

extends equally to phenol derivatives and carboxylic acids. In each case, the ^{31}P NMR resonance and $^1J_{P–H}$ coupling constant fall within a narrow range (−23.5 ppm > δ > 38.3 ppm, 578 Hz < J < 652 Hz) indicative of a homologous structural set of pentacoordinate adducts.

2.2.2. Oxidative Addition of N–H Compounds. Exposure of **2** to primary amines similarly leads to intermolecular N–H oxidative addition. For instance, reaction of **2** with *n*-propylamine, benzylamine, and *tert*-butylamine all lead cleanly to the corresponding hydridoamidophosphoranes (Figure 7). Arylamines, including sterically hindered 2,6-disubstituted anilines, are likewise reactive (viz., **2**·[H][NHDipp]). As with the O–H oxidative addition adducts above, the spectral characteristics of the suite of N–H addition products fall within narrow bounds. However, in contrast to the O–H oxidative addition adducts, the ^{31}P chemical shifts of the N–H oxidative addition products **2**·[H][NHR] are displaced to higher field (−31.4 ppm > δ > −47.4 ppm), consistent with greater nuclear shielding of phosphorus from the more electron-rich addend amide. Relatedly, the coupling constants for **2**·[H][NHR] are ca. 70–80 Hz smaller in magnitude than those of **2**·[H][OR].

Treatment of compound **2** with ammonia results in the formation of a phosphorus-containing product (δ −45.5 ppm, $^1J_{P–H}$ = 521 Hz) consistent with the formulation as oxidative addition product **2**·[H][NH_2]. However, isolation of this compound in pure form has been consistently hampered by the formation of an impurity (δ −51.2 ppm, $^1J_{P–H}$ = 536 Hz)

dx.doi.org/10.1021/ja510558d | J. Am. Chem. Soc. 2014, 136, 17634–17644

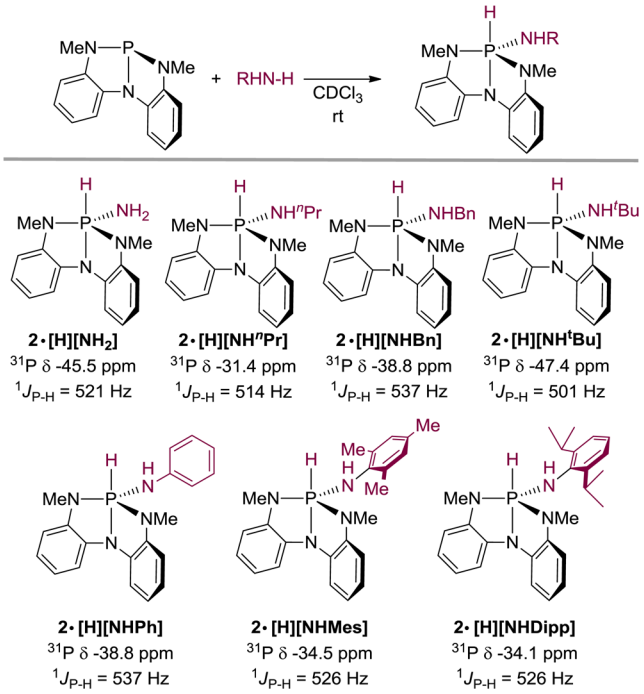

Figure 7. Examples of N−H oxidative addition to **2**, including key ^{31}P NMR parameters.

that we tentatively assign on the basis of mass spectrometry as the dinuclear phosphorane with bridging amido {**2**·[H]}$_2$(μ-NH) that would arise from condensation of 2 equiv of **2**·[H][NH$_2$] with elimination of ammonia.

2.2.3. Solid-State Structures of O−H and N−H Adducts of ***2****.* A variety of O−H and N−H adducts of **2** may be crystallized from chloroform by either concentration of a cooled solution or slow diffusion of pentane via layering. Representative examples (**2**·[H][OPh] and **2**·[H][NHPh]) are depicted in Figure 8, and

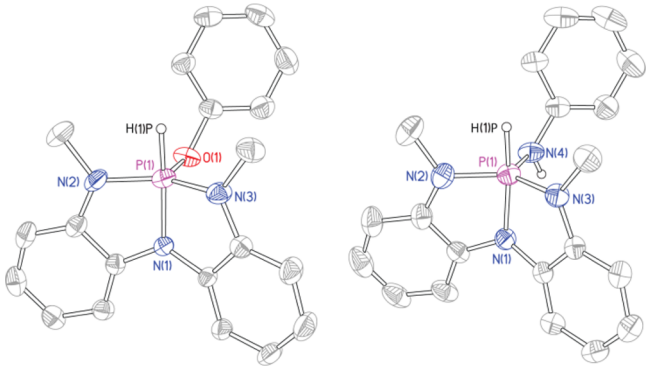

Figure 8. Representative molecular structures of O−H and N−H adducts. ORTEP diagrams of **2**·[H][OPh] (left) and **2**·[H][NHPh] (right) are shown at the 50% probability level. All carbon-based hydrogen atoms and solvent molecules are omitted for clarity.

a tabulation of relevant structural metrics for an extended series of adducts is given in Table 2. In each case, the phosphorus-bound addend hydrogen was located in the difference Fourier map and refined isotropically.

In contrast to the planar meridional chelation of the triamide motif in trigonal bipyramidal **2**·[Cl]$_2$, each of the O−H and N−H adducts **2**·[H][E] retains significant folding along the P$_1$−N$_1$ axis as in tricoordinate **2**. Moreover, with respect to the diarylamido nitrogen, the hydride ligand forms broad obtuse angles ($\angle$H$_1$−P$_1$−N$_1$ ≈ 167°−176°), whereas the addend heteroatom is situated nearly orthogonally ($\angle$N$_1$−P$_1$−E ≈ 91°−96°). Consequently, the overall molecular geometry of the pentacoordinate adducts is best described as distorted structures residing along the continuum between trigonal bipyramidal and square pyramidal. In each structure, the addend heteroatom occupies the position in the pentacoordinate adducts corresponding to the pivot ligand for pseudorotation between trigonal bipyramidal and square pyramidal structures. To a first approximation, we surmise that the observed configurations are preferred primarily on steric grounds, with the small hydride disposed in the more sterically congested position than the addend heteroatom. The importance of steric strain is evident in the suite of aniline adducts, where the increasing steric profile of the addend anilide results in an increase in trigonal bipyramidal character as quantified by the τ values[32] (**2**·[H][NHPh], 0.62; **2**·[H][NHMes], 0.77; **2**·[H][NHDipp], 0.81).

Additional electronic factors further control the precise position along the pseudorotation coordinate, with the identity of the addend heteroatom playing a significant role. For instance, phenol adduct **2**·[H][OPh] tends toward square planar (τ = 0.38), whereas aniline adduct **2**·[H][NHPh] is more trigonal bipyramidal (τ = 0.62). This result can be rationalized by considering the effects of negative hyperconjugation (n → σ*) as substantiated by NBO second-order perturbative energy analysis (Table 3). The stabilization energy arising from delocalization of lone pair density on the *N*-methylanilides into the antibonding orbital σ*(P−E) is greater for **2**·[H][OPh] than **2**·[H][NHR]. This difference is mainly attributable to the $\varepsilon_a - \varepsilon_d$ term (the energy separation between the donor and acceptor orbitals), which is smaller for donation into the σ*(P−O) orbital of **2**·[H][OPh]. Simultaneously, lone pair density on the more electronegative phenolate oxygen atom is itself less energetically available for negative hyperconjugation into σ*(P−N$_2$) and σ*(P−N$_3$). The consequence of these synergistic effects is a broadening of the angle $\angle$N$_2$−P$_1$−N$_3$ due to n(N) → σ*(P−O) interaction in **2**·[H][OPh] that drives it toward a square pyramidal geometry. The observation that oxyphosphoranes **2**·[H][OR] favor square pyramidal structures and amidophosphoranes **2**·[H][NHR] favor trigonal bipyramidal structures appears to be general for the suite of compounds that we have been able to successfully characterize in the solid state (see Table 2).

2.3. Mechanistic Considerations. *2.3.1. In Situ Spectroscopic Observations.* A stepwise mechanistic course for the E−H oxidative addition reactions at **2** has been detected by ^{31}P NMR spectroscopy. The reaction of **2** with *p*-methoxyphenol illustrates the generally observed behavior. When 1 equiv of *p*-methoxyphenol was added to a CDCl$_3$ solution of **2** in a sealable NMR tube, the signal for **2** (δ 159.8 ppm) was consumed within minutes and replaced by two singlet ^{31}P resonances at δ 119.7 ppm and δ 110.7 ppm in a ∼1:1 ratio (see the Supporting Information for the spectra). Over the course of several hours, continued monitoring of the reaction mixture at ambient temperature then witnessed the full conversion of these intermediates to the final phosphorane product (δ −23.5 ppm). The formation and consumption of intermediates in this fashion is general for all of the O−H and N−H oxidative addition reactions we have investigated.

In situ monitoring of the addition of *tert*-butyl alcohol to **2** permits an assessment of the identity of these intermediates. As

dx.doi.org/10.1021/ja510558d | J. Am. Chem. Soc. 2014, 136, 17634−17644

Table 2. Tabulated Bond Distances (Å), Angles (deg), and τ Values for Selected Adducts 2·[H][ER][a]

metric	2·[H][OPh]	2·[H][OBz]	2·[H][O^{t}Bu]	2·[H][NHPh]	2·[H][NHMes]	2·[H][NHDipp]
d(P$_1$–N$_1$)	1.765(2)	1.7645(14)	1.7773(12)	1.788(3)	1.792(2)	1.7863(18)
d(P$_1$–N$_2$)	1.697(3)	1.6796(14)	1.6985(12)	1.701(3)	1.701(2)	1.6994(19)
d(P$_1$–H$_1$)	1.34(2)	1.310(16)	1.319(15)	1.34(3)	1.36(2)	1.32(2)
d(P$_1$–E)	1.657(2)	1.6908(12)	1.6129(9)	1.687(4)	1.660(2)	1.6637(19)
∠N$_1$–P$_1$–E	95.55(11)	94.63(7)	92.08(5)	94.49(16)	92.73(11)	91.16(9)
∠H$_1$–P$_1$–N$_1$	167.6(10)	170.7(8)	170.0(6)	169.5(14)	173.9(9)	175.5(9)
∠N$_2$–P$_1$–N$_3$	144.65(13)	145.29(7)	136.91(6)	132.20(16)	127.97(11)	126.64(10)
τ[b]	0.38	0.42	0.55	0.62	0.77	0.81

[a]See the Supporting Information for full crystallographic details. [b]τ = (∠H$_1$–P$_1$–N$_1$ — ∠N$_2$–P$_1$–N$_3$)/60.

Table 3. NBO Second-Order Perturbation Energy Analysis for 2·[H][OPh] and 2·[H][NHPh][a]

donor[b]	acceptor[b]	ΔE[c]	$\varepsilon_a - \varepsilon_d$[d]	F_{da}[e]
	2·[H][OPh]			
n(N$_2$)	σ*(P–OPh)	13.39	0.47	0.071
n(N$_3$)	σ*(P–OPh)	13.39	0.47	0.071
n(OPh)	σ*(P–N$_2$)	6.78	0.70	0.061
n(OPh)	σ*(P–N$_3$)	6.78	0.70	0.061
	2·[H][NHPh]			
n(N$_2$)	σ*(P–NHPh)	11.18	0.52	0.068
n(N$_3$)	σ*(P–NHPh)	10.72	0.52	0.067
n(NHPh)	σ*(P–N$_2$)	9.11	0.63	0.067
n(NHPh)	σ*(P–N$_3$)	7.48	0.64	0.062

[a]Structures optimized at the B3LYP/6-311+G** level. [b]N$_2$ and N$_3$ are the *N*-methylanilides of the triamide ligand. [c]Stabilization energy of donor–acceptor interaction, kcal/mol. [d]Donor–acceptor orbital energy difference, au. [e]Off-diagonal NBO Fock matrix element.

with *p*-methoxyphenol, addition of *tert*-butyl alcohol to **2** results in the initial formation of two singlet signals (δ 117.7 ppm and δ 110.8 ppm, relative ratio ~2:1) which then proceed on to **2**·[H][O^{t}Bu] (δ −37.5 ppm) in >95% NMR conversion. Diffusion of pentane by layering onto this chloroform solution deposits X-ray-quality crystals that are confirmed to be pentacoordinate phosphorane **2**·[H][O^{t}Bu] by diffraction. Immediately upon redissolution of this single-crystalline sample in $CDCl_3$, the sole observable ^{31}P NMR resonance is that of **2**·[H][O^{t}Bu] at δ −37.5 ppm. However, over the course of 1 h, the two singlets at δ 117.7 ppm and δ 110.8 ppm are again observed with the same ~2:1 ratio. The intensity of these signals was found to vary with respect to that of **2**·[H][O^{t}Bu] as a function of temperature in a reversible fashion (Figure 9), permitting a thermodynamic assessment of the equilibrium by van't Hoff analysis in the temperature range from −10 to +40 °C. From this correlation, the values of ΔH = +4.5(1) kcal/mol and ΔS = +13.8(5) cal/(mol·K) were extracted.

The ^{31}P chemical shifts of the observed intermediates do not exhibit $^1J_{P-H}$ coupling and fall in a range consistent with those expected for tricoordinate phosphorodiamidites of the general formula P(OR)(NR)$_2$.[33] Taken together with the thermodynamic parameters that show only a modest entropy change in the equilibrium, we postulate the unimolecular σ^3-P ⇌ σ^5-P ring–chain tautomerism[34] depicted in eq 3 as the most likely explanation for the observed equilibrium behavior. We assign the major diastereomer (δ 117.7 ppm) as *anti*-**5** on the basis of steric considerations.

The implication of these observations is that the observed oxidative addition reactions to **2** proceed via a stepwise mechanism involving initial E–H bond cleavage by phosphorus–ligand cooperativity, followed by subsequent intramolecular σ^3-P → σ^5-P tautomerism.

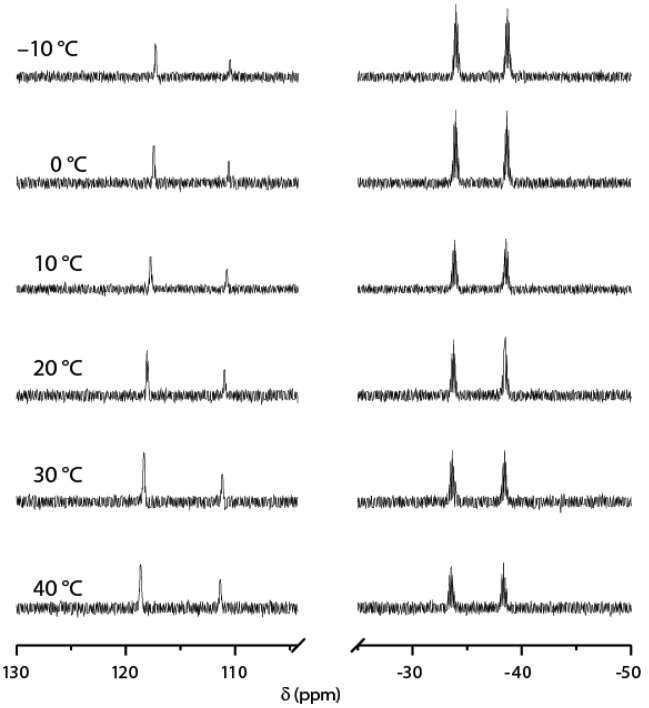

Figure 9. Variable-temperature (−10 °C < T < +40 °C) proton-coupled ^{31}P NMR of **2**·[H][O^{t}Bu] showing the ring–chain equilibrium in eq 3. The signal for **2**·[H][O^{t}Bu] (δ −37.5 ppm) shows proton coupling.

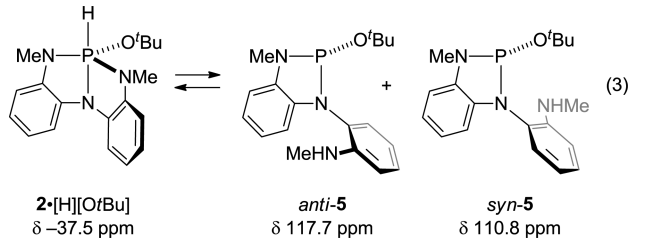

2.3.2. Exchange Equilibria and Substituent Effects. To the extent that the above results suggest partial reversibility in the formation of the pentacoordinate phosphorane adducts, we were interested in assessing the potential for ligand exchange for adducts **2**·[H][E]. Both O–H and N–H adducts of **2** are found to undergo exchange by treatment with exogenous phenols and anilines in solution at room temperature over the course of several days. Conducting these exchange experiments with a panel of *para*-substituted phenols and anilines permitted

dx.doi.org/10.1021/ja510558d | J. Am. Chem. Soc. 2014, 136, 17634–17644

an evaluation of substituent effects. The equilibrium constants for the equilibria indicated in eqs 4 and 5 were measured by ^{1}H NMR spectroscopy in chloroform-*d* solution; the data are tabulated in Table 4.

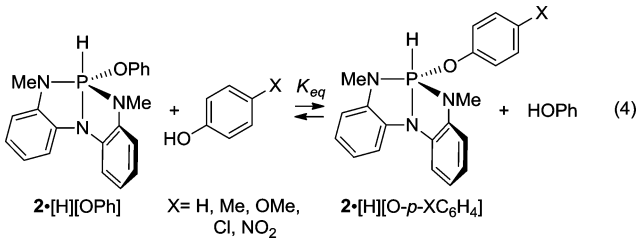

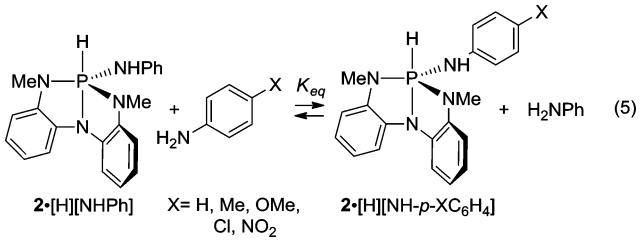

Table 4. Equilibrium Constants for Exchange Reactions in Eqs 4 and 5

entry	substrate	−X	K_{eq} [a]	ΔG° (kcal/mol)
1	2·[H][OPh]	−OMe	1.34	−0.17
2	2·[H][OPh]	−Me	1.28	−0.14
3	2·[H][OPh]	−Cl	0.95	+0.03
4	2·[H][OPh]	−NO$_2$	0.22	+0.90
5	2·[H][NHPh]	−OMe	2.98	−0.65
6	2·[H][NHPh]	−Me	1.91	−0.38
7	2·[H][NHPh]	−Cl	0.95	+0.03
8	2·[H][NHPh]	−NO$_2$	0.18	+1.01

[a]Determined by ^{1}H NMR spectroscopy at room temperature.

Qualitatively, the results of these equilibrium exchange experiments establish that, within a given heteroatom series, the phosphorane adducts are stabilized by the incorporation of more electron-donating *para*-substituents relative to *p*-H. This finding is quantified by Hammett analysis; linear correlations were obtained for the relationships of log(K_{eq}) vs σ_p^-, with sensitivity factors ρ = −0.52 for the phenol series (Figure 10) and ρ = −0.72 for the aniline series (Figure 11).

Treatment of amidophosphorane 2·[H][NHPh] with 1 equiv of phenol results in quantitative conversion to oxyphosphorane 2·[H][OPh] with loss of aniline. The equilibrium constant for this exchange reaction was estimated by ^{1}H NMR at $K_{eq} > 10^4$, indicating the proclivity of the phosphorane to accommodate the phenolate substituent in preference to the anilide. This observation, which parallels results in related hypervalent main group systems,[35] indicates a significant electrostatic contribution to the polar covalent bonding in these phosphorane molecules.

2.3.3. O−H and N−H Reductive Elimination from 2. We have established that the O−H and N−H oxidative addition reactions to **2** are reversible in certain circumstances. Specifically, when pentacoordinate adducts 2·[H][O^{t}Bu] and 2·[H][NH^{t}Bu] (prepared by oxidative addition of *tert*-butyl alcohol and *tert*-butylamine, respectively) are heated to reflux in

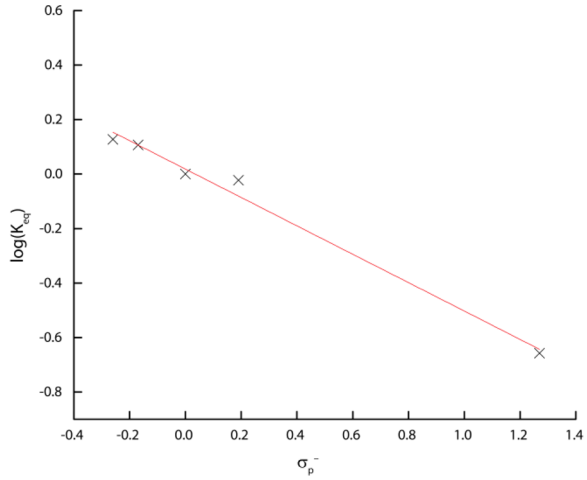

Figure 10. Hammett plot (ρ = −0.52) of the phenol exchange equilibria depicted in eq 4.

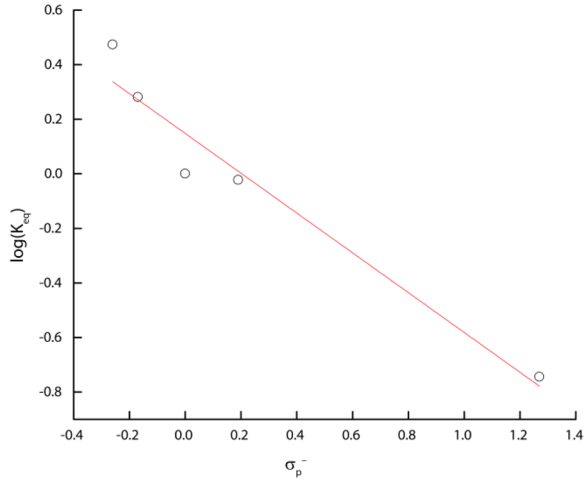

Figure 11. Hammett plot (ρ = −0.72) of the aniline exchange equilibria depicted in eq 5.

toluene under a dynamic nitrogen sweep, tricoordinate compound **2** is obtained by reductive elimination (eq 6). In

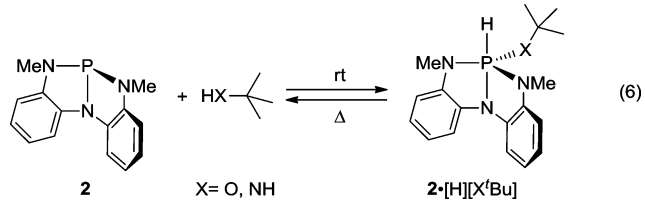

the case of 2·[H][NH^{t}Bu], this conversion is quantitative; in the case of 2·[H][O^{t}Bu], the yield of **2** is ca. 30%, with the balance of phosphorus-containing material remaining as 2·[H][O^{t}Bu] presumably due to inefficient removal of *tert*-butyl alcohol from the reaction vessel.

3. DISCUSSION

In both its structure and reactivity, compound **2** is an unusual σ^3-P compound that illustrates the extent to which molecular distortion in the main group leads to noncanonical behavior. In addition to its markedly nontrigonal ground state, **2** displays dynamic conformational behavior arising from a low-energy inversion at phosphorus. The energetic barrier to inversion at **2**

dx.doi.org/10.1021/ja510558d | J. Am. Chem. Soc. 2014, 136, 17634−17644

($\Delta G_{exptl}^{\ddagger}$ = +10.7(5) kcal/mol, $\Delta G_{calcd}^{\ddagger}$ = +5.7 kcal/mol) is anomalously low when compared to that of 3-fold-symmetric heteroatom-substituted σ^3-P compounds;[36] the presence of lone-pair-containing substituents on phosphorus is expected to lead to large barriers to inversion due to pπ−pπ repulsion in the planar Y-shaped transition structures. This apparent anomaly is resolved by DFT calculations which implicate a stepwise edge-inversion mechanism proceeding though a C_2-symmetric T-shaped conformer. By transiting through a T-shaped structure, repulsive interactions between lone pairs on adjacent atoms are eliminated as the phosphorus presents a vacant 3p orbital with appropriate symmetry for stabilizing overlap with the substituent nitrogen lone pairs. In subtle contrast to the edge-inversion process first proposed by Arduengo, our computed mechanism finds the C_2-symmetric T-shaped conformer as a local minimum, as opposed to a first-order saddle point, along the inversion coordinate.

The connection between edge inversion of tricoordinate compounds and Berry pseudorotation of pentacoordinate compounds has been previously noted by Arduengo.[37] With respect to platform **2**, the conformational flexibility of the tricoordinate state is also evident in the pentacoordinate state, where the triamide ligand architecture is sufficiently flexible to support phosphorane structures that span the pseudorotation coordinate.[38] As an illustrative example, trigonal bipyramidal **2**·$[Cl]_2$ positions its *N*-methylanilide substituents in *trans* diaxial positions, whereas trigonal bipyramidal **2**·[H][NHDipp] positions its *N*-methylanilide substituents in *cis* diequatorial positions (Figure 12).

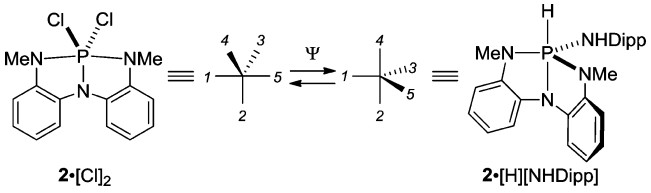

Figure 12. Illustration of σ^5-P structures that span the pseudorotation coordinate.

Evidently, the observed conformation at phosphorus is sensitive to the identity of the acyclic substituents, and distorted pentacoordinate structures intermediate along the pseudorotation coordinate are observed for adducts **2**·[H][E]. We infer that an interplay between steric effects and negative hyperconjugation is responsible for the precise molecular structure adopted.[39] The effect of negative hyperconjugation may further be related to the observed trend in $^1J_{P-H}$ coupling constant for **2**·[H][OR] and **2**·[H][NHR]. In driving the hydride ligand into a more rigorously apical position, a decrease in the phosphorus-based s-orbital content of the three-center, four-electron ω-bond[40] containing the hydride would be expected.[41] This effect, which should decrease the observed $^1J_{P-H}$ coupling constants, would be maximized for the amidophosphoranes **2**·[H][NHR], which exhibit the greatest trigonal bipyramidal character. This interpretation is not exclusive of the possibility that compounds **2**·[H][E] remain conformationally dynamic in solution, undergoing low-energy pseudorotation in which the hydride samples various coordination sites.

With respect to reactivity, the molecular deformation imposed by the chelating triamide ligand leads to an electronic rehybridization at phosphorus that significantly increases the s-character of the lone pair. The nucleophilicity of **2** is therefore unusually low for a phosphorous triamide. Complementarily, the folded arrangement of the triamide presents **2** in a geometry approximating a *cis*-divacant trigonal bipyramid that predisposes the phosphorus to the formation of stable phosphoranes. In effect, geometrically constrained compound **2** may be viewed as an entatic state[42] of phosphorus en route from σ^3-P to σ^5-P, such that the intermolecular reaction **2** + E−H → **2**·[H][E] is exergonic at room temperature.

The stability of the pentacoordinate structures reported here bears a relationship to other known phosphorus compounds. Contreras has reported related *O,N,O*-chelated phosphoranes, including several stable hydridophosphoranes.[43] Lattman has described phosphorus compounds constrained within calix[4]-arenes.[44] Phosphoranes with apical hydrides have been reported by Martin,[45] Verkade,[46] and Kawashima.[47]

Mechanistically, the intermolecular E−H oxidative addition reactions studied here proceed via a stepwise pathway involving phosphorus−ligand cooperativity. The observed cooperative behavior of **2** is analogous to related reactivity of electrophilic group 13[48] and group 14[49] compounds and finds extensive precedent in mechanistic proposals for the phosphorylation of protic pronucleophiles with σ^3-P amide reagents.[50] There is, however, a distinction with respect to previous mechanistic work on E−H oxidative addition at electrophilic σ^3-P compounds. For instance, we have shown that N−H oxidative addition to **1** proceeds in a stepwise fashion that is initiated by amine binding to the electrophilic phosphorus center and requires additional equivalencies of amine to serve as a mediator for N → P prototropy.[17] We speculate that, in the case of **2**, the *N*-methylanilide substituents play the role of proton shuttle, such that initial Lewis acid−base adduct **6** evolves by intramolecular proton transfer to give diastereomers *anti*-**7** and *syn*-**7** (Figure 13), which subsequently undergo

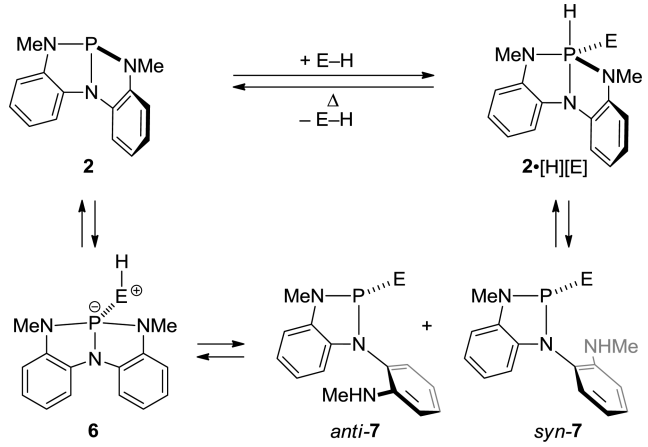

Figure 13. Proposed stepwise mechanism for E−H oxidative addition to **2**.

intramolecular σ^3-P → σ^5-P ring−chain tautomerism[34] of the type that has been well-documented to furnish the observed pentacoordinate adduct **2**·[H][E]. The importance of ring strain in facilitating electrophilic reactivity at σ^3-P has been discussed by Hudson.[51]

Whereas the requirement for an exogenous proton shuttle prohibited E−H reductive elimination from isolated **1**·[H]-[E],[17] isolated σ^5-P compounds **2**·[H][E] are shown to revert to σ^3-P and free E−H by thermolysis in solution. Such reversibility for E−H oxidative addition is rare for main group

dx.doi.org/10.1021/ja510558d | J. Am. Chem. Soc. 2014, 136, 17634−17644

systems[52] and indicates that compounds of type **2** may be energetically well-poised to participate in reversible bond activation that may ultimately be leveraged for E−H functionalization chemistry.

4. SUMMARY

The geometrically distorted compounds **2** and **4** presented here represent well-characterized examples of nontrigonal σ^3-P species. The geometry enforced by the triamide ligand leads to local C_s symmetry at phosphorus, with an increase in lone pair s-character that results in unusual reactivity and remarkable conformational flexibility. In contrast to canonical 3-fold-symmetric σ^3-P structures, the phosphorus center of **2** is poorly nucleophilic but instead undergoes intermolecular oxidative addition of O−H and N−H bonds to give stable σ^5-P compounds. While questions regarding the kinetics and stereochemistry of oxidative addition to **2** remain at this juncture, these reactions are believed to proceed via a ligand cooperative mechanism on the basis of in situ ^{31}P NMR observations. Solid-state structural analysis in conjunction with computational results implicates negative hyperconjugation as a major factor governing the relative stability and structure of σ^5-P adducts **2**·[H][E]. In contrast to the geometrically distorted compound **1**, oxidative additions to **2** are reversible at elevated temperatures. Consequently, the potential for **2** to promote novel transformations of small molecules via bond activation remains an ongoing area of interest. Additional efforts are also being directed to the synthesis of alternative low-symmetry σ^3-P compounds for the oxidative addition of even less reactive, nonpolar covalent bonds.

5. EXPERIMENTAL SECTION

A full description of the general experimental methods, including preparation and purification of starting materials, can be found in the Supporting Information.

5.1. Synthesis. *5.1.1. Compound 2.* Phosphorus trichloride (1.68 mL, 19.3 mmol) was dissolved in a 1:1 mixture of THF (55 mL) and ether (55 mL) and cooled to −78 °C. A solution of triamine **3a** (4.39 g, 19.3 mmol) in THF (36 mL) was added dropwise via syringe. When the addition was complete, triethylamine (8.2 mL, 58.8 mmol) in ether (36 mL) was added slowly via syringe. The reaction mixture was stirred at −78 °C for 1 h and then warmed to room temperature. After 4 h, the white precipitate was removed via filtration, and the solvent was removed in vacuo. The resulting brick red solid was then dissolved in a minimum amount of ether at room temperature. The saturated solution was filtered through a pad of Celite and then cooled in a freezer (ca. −35 °C) to yield the title phosphorus compound as off-white crystals (3.94 g, 80%). ^{1}H NMR ($CDCl_3$, 400 MHz): δ 7.50 (d, 2H, J = 7.6 Hz), 7.09 (t, 2H, J = 7.6 Hz), 6.90 (t, 2H, J = 7.6 Hz), 6.66 (d, 2H, J = 7.5 Hz), 3.12 (d, 6H, J = 8.4 Hz) ppm. ^{13}C NMR ($CDCl_3$, 100 MHz): δ 141.2 (d, $^2J_{P-C}$ = 7.1 Hz), 139.5, 124.3, 118.9, 117.0 (d, $^2J_{P-C}$ = 5.9 Hz), 108.6, 29.8 (d, $^2J_{P-C}$ = 30.6 Hz) ppm. ^{31}P NMR ($CDCl_3$, 145 MHz): δ 159.77 ppm. MS (ESI) m/z calcd for $C_{14}H_{15}N_3P$ (M + H) 256.1004, found 256.0998.

5.1.2. Compound 4. To a solution of PCl_3 (0.44 mL, 5.0 mmol) in pentane (25 mL) under N_2 at −78 °C was added triamine ligand **3b** (1.41 g, 5.0 mmol) in pentane (25 mL) dropwise via syringe. Triethylamine (2.1 mL, 15.0 mmol) in pentane (10 mL) was then added dropwise, and the resulting mixture was warmed to room temperature and stirred for an additional 2.5 h, giving a white suspension within a light yellow solution. The reaction mixture was filtered by cannula, and the filtrate was concentrated to a light yellow solid. The solid was redissolved in ca. 90 mL of pentane, and an insoluble white precipitate was removed via canula filtration. The filtrate was again concentrated to give white solids, which could be further recrystallized from a concentrated pentane solution at −35 °C to give **4** as colorless crystals (1.26 g, 83%). ^{1}H NMR ($CDCl_3$, 360 MHz): δ 7.39 (d, 2H, J = 7.9 Hz), 6.95 (dt, 2H, J = 8.3 Hz, J = 1.1 Hz), 6.76 (dt, 2H, J = 8.3 Hz, J = 1.1 Hz), 6.68 (d, 2H, J = 7.6 Hz), 4.07−3.97 (m, 2H), 1.51 (d, 12H, J = 6.8 Hz) ppm. ^{13}C NMR ($CDCl_3$, 90 MHz): δ 141.8 (d, J_{P-C} = 6.3 Hz), 138.0, 123.9, 118.5, 117.5 (d, J_{P-C} = 6.3 Hz), 110.4, 46.9 (d, $^2J_{P-C}$ = 22.5 Hz), 22.0 (d, $^3J_{P-C}$ = 7.2 Hz) ppm. ^{31}P NMR ($CDCl_3$, 145 MHz): δ 151.72 ppm. MS (ESI) m/z calcd for $C_{18}H_{23}N_3P$ (M + H) 312.1630, found 312.1628.

5.1.3. Compound 2·[Cl]$_2$. A solution of triamine ligand **3a** (3.64 g, 16.0 mmol) in 32 mL of CH_2Cl_2 was added dropwise to phosphorus pentachloride (3.34 g, 16.0 mmol) in 67 mL of CH_2Cl_2 at −78 °C under nitrogen. When the addition was complete, triethylamine (6.7 mL, 48.0 mmol) in 12 mL of CH_2Cl_2 was added dropwise. The mixture was warmed slowly to room temperature and stirred overnight. Removal of the volatiles in vacuo left a green solid which was triturated with pentane. After filtration, the pentane filtrate was concentrated to yield a green solid (3.86 g, 74%). The product was recrystallized from pentane to yield light yellow-green crystals. ^{1}H NMR ($CDCl_3$, 360 MHz): δ 7.88 (d, 2H, J = 8.0 Hz), 7.17−7.12 (m, 2H), 7.04−6.99 (m, 2H), 6.81 (d, 2H, J = 7.8 Hz), 3.34 (d, 6H, J = 19.2 Hz) ppm. ^{13}C NMR ($CDCl_3$, 90 MHz): δ 135.5 (d, J_{P-C} = 15.8 Hz), 124.3 (d, J_{P-C} = 20.4 Hz), 122.9 (d, J_{P-C} = 1.2 Hz), 118.7 (d, J_{P-C} = 1.9 Hz), 112.0 (d, J_{P-C} = 11.0 Hz), 107.0 (d, J_{P-C} = 11.0 Hz), 33.6 (d, $^2J_{P-C}$ = 5.2 Hz) ppm. ^{31}P NMR ($CDCl_3$, 145 MHz): δ −32.44 ppm.

5.1.4. Compound 2·[H][OPh]. To a solution of σ^3-P compound **2** (50 mg, 0.20 mmol, 1 equiv) in dry $CDCl_3$ (0.5 mL) was added a solution of phenol (18 mg, 0.20 mmol, 1 equiv) in dry $CDCl_3$ (0.5 mL). The solution was then stirred and monitored by ^{31}P NMR until complete conversion to product was observed (ca. 2 h). Solids obtained by removal of the solvent in vacuo were further purified by slow diffusion (layering) of pentane to a chloroform solution in a −35 °C freezer to yield white crystals. ^{1}H NMR ($CDCl_3$, 400 MHz): δ 7.61 (d, 2H, J = 6.8 Hz), 7.22 (t, 2H, J = 6.8 Hz), 7.07−7.03 (m, 5H), 6.90−6.86 (m, 2H), 6.70 (d, 2H, J = 7.6 Hz), 6.33 (d, 1H, $^1J_{P-H}$ = 615 Hz), 3.10 (d, 6H, $^3J_{P-H}$ = 17.6 Hz) ppm. ^{13}C NMR ($CDCl_3$, 100 MHz): δ 151.8 (d, J_{P-C} = 7.6 Hz), 132.0 (d, J_{P-C} = 11.9 Hz), 131.1 (d, J_{P-C} = 16.7 Hz), 129.3 (d, J_{P-C} = 3.1 Hz), 124.1 (d, J_{P-C} = 3.4 Hz), 122.3 (d, J_{P-C} = 5.4 Hz), 120.2 (s), 119.6 (d, J_{P-C} = 1.3 Hz), 110.7 (d, J_{P-C} = 11.1 Hz), 108.9 (d, J_{P-C} = 7.6 Hz), 28.5 (d, J_{P-C} = 17.6 Hz) ppm. ^{31}P NMR ($CDCl_3$, 145 MHz): δ −24.54 (d heptet, $^1J_{P-H}$ = 614 Hz, $^3J_{P-H}$ = 17.5 Hz) ppm. MS (ESI) m/z calcd for $C_{20}H_{20}N_3OP$ (M + H) 350.1422, found 350.1415.

5.1.5. Compound 2·[H][NHPh]. To a solution of σ^3-P compound **2** (50 mg, 0.20 mmol, 1 equiv) in dry $CDCl_3$ (0.5 mL) was added a solution of aniline (18 μL, 0.20 mmol, 1 equiv) in dry $CDCl_3$ (0.5 mL). The solution was then stirred and monitored by ^{31}P NMR until complete conversion to product was observed (ca. 2 h). Solids obtained by removal of the solvent in vacuo were further purified by slow diffusion (layering) of pentane to a chloroform solution in a −35 °C freezer to yield white crystals. ^{1}H NMR (400 MHz, $CDCl_3$): δ 7.44 (d, 2H, J = 7.2 Hz), 7.16 (t, J = 7.0 Hz), 7.00−6.90 (m, 5H), 6.73 (s, 4H), 6.33 (dd, 1H, $^1J_{P-H}$ = 540 Hz, J = 7.2 Hz), 4.19 (d, 1H, J = 6.4 Hz), 3.08 (d, 6H, $^3J_{P-H}$ =16.8 Hz) ppm. ^{13}C NMR (75 MHz, $CDCl_3$): δ 133.6 (d, J_{P-C} =14.8 Hz), 133.6 (d, J_{P-C} =13.7 Hz), 129.4 (s), 122.3 (d, J_{P-C} =1.7 Hz), 121.6 (d, J_{P-C} =7.7 Hz), 121.1 (s), 119.6 (d, J_{P-C} = 1.2 Hz), 115.5 (s), 111.8 (d, J_{P-C} =10.3 Hz), 109.2 (d, J_{P-C} = 8.0 Hz), 29.6 (d, J_{P-C} = 16.3 Hz) ppm. ^{31}P NMR (146 MHz, $CDCl_3$): δ −38.8 (d septet, $^1J_{P-H}$ = 536.5 Hz, $^3J_{P-H}$ = 16.1 Hz) ppm. Anal. Calcd (Found) for $C_{20}H_{21}N_4P$: C, 68.95 (68.43); H, 6.08 (5.71); N, 16.09 (16.03); P, 9.18 (8.98).

5.2. Variable-Temperature NMR Spectroscopy of 4. In an inert atmosphere glovebox, compound **4** (30 mg) was dissolved in THF-d_8 (1 mL). The sample was then transferred to a sealable J-Young NMR tube. Variable-temperature NMR experiments were recorded on a Bruker DPX-300 spectrometer. ^{1}H and ^{31}P NMR spectra were recorded at temperature intervals between T < −20 °C and T > −80 °C. The sample and probe were thermostated at each temperature for 5 min before the spectra were recorded. At the end of

the experiment, a spectrum at room temperature was recorded to verify the reversibility of the temperature-dependent process. Line shape fitting was performed using the WinDNMR software package.[53] All chemical shifts, coupling constants, and line width values were set on the basis of values derived from the experimental spectra. The exchange rate variable was adjusted to fit the overlaid experimental spectrum at each temperature.

5.3. Computational Methods. Geometries were optimized in Gaussian 09[54] using the B3LYP[55] density functional with the 6-311+G(d,p) basis set. Geometry optimizations were performed in the gas phase without symmetry constraint. Stationary points were characterized by frequency calculations to confirm their identity as either local minima (zero imaginary frequencies) or first-order saddle points (one imaginary frequency). For transition structure 2TS, an intrinsic reaction coordinate (IRC) calculation was conducted to ensure connection along the potential energy surface to **2**. See the Suporting Information for full details.

■ ASSOCIATED CONTENT

Supporting Information

Full experimental procedures, ^{1}H, ^{13}C, and ^{31}P NMR spectra for all synthetic compounds, ^{1}H VT-NMR spectra of **4** including spectral simulations, crystallographic details, computational methods, Cartesian coordinates, and X-ray crystallographic data in CIF format. This material is available free of charge via the Internet at http://pubs.acs.org.

■ AUTHOR INFORMATION

Corresponding Author

radosevich@psu.edu

Notes

The authors declare no competing financial interest.

■ ACKNOWLEDGMENTS

The synthesis and characterization of tricoordinate phosphorus compounds were supported by the National Science Foundation under Award CHE-1352164. Additional financial support was provided by The Pennsylvania State University. A.T.R. gratefully acknowledges early career support from the Alfred P. Sloan Foundation. We thank Dr. Sunewang Rixin Wang for preliminary synthetic work.

■ REFERENCES

(1) Hudson, R. F. *Structure and Mechanism in Organophosphorus Chemistry*; Academic Press: New York, 1965.

(2) Gilheany, D. G. *Chem. Rev.* **1994**, *94*, 1339.

(3) Cadogan, J. I. G. *Organophosphorus Reagents in Organic Synthesis*; Academic Press: London, New York, 1980.

(4) Kamer, P. C. J.; van Leeuwen, P. W. N. M. *Phosphorus(III) Ligands in Homogeneous Catalysis: Design and Synthesis*; Wiley: Hoboken, NJ, 2012.

(5) (a) Methot, J. L.; Roush, W. R. *Adv. Synth. Catal.* **2004**, *346*, 1035. (b) Fan, Y. C.; Kwon, O. *Chem. Commun.* **2013**, *49*, 11588.

(6) (a) Burdett, J. K. *Molecular Shapes*; Wiley-Interscience: New York, 1980; pp 54–58. (b) Pearson, R. G. *J. Mol. Struct.: THEOCHEM* **1983**, *103*, 25.

(7) Albright, T. A.; Burdett, J. K.; Whangbo, M.-H. *Orbital Interactions in Chemistry*; Wiley-Interscience: New York, 1985.

(8) (a) Baechler, R. D.; Mislow, K. *J. Am. Chem. Soc.* **1970**, *92*, 3090. (b) Baechler, R. D.; Mislow, K. *J. Am. Chem. Soc.* **1970**, *92*, 4758. (c) Mislow, K.; Baechler, R. D. *J. Am. Chem. Soc.* **1971**, *93*, 773. (d) Mislow, K.; Egan, W. *J. Am. Chem. Soc.* **1971**, *93*, 1805.

(9) (a) Driess, M.; Merz, K.; Monsé, C. *Z. Anorg. Allg. Chem.* **2000**, *626*, 2264. (b) Marque, S.; Tordo, P. *Top. Curr. Chem.* **2005**, *250*, 43–76. (c) Pan, X.; Chen, X.; Li, T.; Li, Y.; Wang, X. *J. Am. Chem. Soc.* **2013**, *135*, 3414.

(10) (a) . (b) Vedejs, E.; Donde, Y. *J. Am. Chem. Soc.* **1997**, *119*, 9293. (c) Wolfe, B.; Livinghouse, T. *J. Am. Chem. Soc.* **1998**, *120*, 5116. (d) Reichl, K. D.; Ess, D. H.; Radosevich, A. T. *J. Am. Chem. Soc.* **2013**, *135*, 9354–9357.

(11) Culley, S. A.; Arduengo, A. J. *J. Am. Chem. Soc.* **1984**, *106*, 1164.

(12) Arduengo, A. J.; Stewart, C. A. *Chem. Rev.* **1994**, *94*, 1215.

(13) Minkin, V. I.; Minyaev, R. M. *Chem. Rev.* **2001**, *101*, 1247.

(14) Arduengo, A. J.; Dixon, D. A. In *Heteroatom Chemistry*; Block, E., Ed.; VCH: New York, 1990; p 47.

(15) For leading references on approaches to nonmetal bond activation and catalysis, see: (a) Power, P. P. *Nature* **2010**, *463*, 171. (b) Martin, D.; Soleilhavoup, M.; Bertrand, G. *Chem. Sci.* **2011**, *2*, 389. (c) Stephan, D. W.; Erker, G. *Angew. Chem., Int. Ed.* **2010**, *49*, 46.

(16) Dunn, N. L.; Ha, M.; Radosevich, A. T. *J. Am. Chem. Soc.* **2012**, *134*, 11330.

(17) McCarthy, S. M.; Lin, Y.-C.; Devarajan, D.; Chang, J. W.; Yennawar, H. P.; Rioux, R. M.; Ess, D. H.; Radosevich, A. T. *J. Am. Chem. Soc.* **2014**, *136*, 4640.

(18) Bouhadir, G.; Bourissou, D. *Chem. Soc. Rev.* **2004**, *33*, 210.

(19) Mitzel, N. W.; Smart, B. A.; Dreihäupl, K.-H.; Rankin, D. W. H.; Schmidbaur, H. *J. Am. Chem. Soc.* **1996**, *118*, 12673.

(20) Cowley, A. H.; Dewar, M. J. S.; Goodman, D. W.; Schweiger, J. R. *J. Am. Chem. Soc.* **1973**, *95*, 6506.

(21) Harvey, R. G.; Schneider, J. F. Hexamethylphosphorous Triamide. *Encyclopedia of Reagents for Organic Synthesis*; John Wiley & Sons, Ltd.: New York, 2001.

(22) Ren, P.; Vechorkin, O.; Allmen, K.; von Scopelliti, R.; Hu, X. *J. Am. Chem. Soc.* **2011**, *133*, 7084.

(23) Nguyen, A. I.; Blackmore, K. J.; Carter, S. M.; Zarkesh, R. A.; Heyduk, A. F. *J. Am. Chem. Soc.* **2009**, *131*, 3307.

(24) NBO 6.0: Glendening, E. D., Badenhoop, J. K., Reed, A. E., Carpenter, J. E., Bohmann, J. A., Morales, C. M., Landis, C. R., and Weinhold, F., Theoretical Chemistry Institute, University of Wisconsin, Madison, WI, 2013.

(25) Prepared by treatment of **2** with elemental selenium. See the Supporting Information for full experimental and characterization details.

(26) Allen, D. W.; Taylor, B. F. *J. Chem. Soc., Dalton Trans.* **1982**, 51–54.

(27) Vogt, H.; Wulff-Molder, D.; Ritschl, F.; Mücke, M.; Skrabei, U.; Meisel, M. *Z. Anorg. Allg. Chem.* **1999**, *625*, 1025.

(28) Kroshefsky, R. D.; Weiss, R.; Verkade, J. G. *Inorg. Chem.* **1979**, *18*, 469.

(29) Rømming, C.; Songstad, J. *Acta Chem. Scand.* **1979**, *33A*, 187.

(30) (a) Dixon, D. A.; Arduengo, A. J.; Fukunaga, T. *J. Am. Chem. Soc.* **1986**, *108*, 2461. (b) Arduengo, A. J.; Dixon, D. A.; Roe, D. C. *J. Am. Chem. Soc.* **1986**, *108*, 6821. (c) Dixon, D. A.; Arduengo, A. J. *J. Chem. Soc., Chem. Commun.* **1987**, 498.

(31) For previous examples of E–H oxidative addition to σ^3-P, see: Pudovik, M. A.; Ovchinnikov, V. V.; Cherkasov, R. A.; Pudovik, A. N. *Russ. Chem. Rev.* **1983**, *52*, 361 and references therein.

(32) Addison, A. W.; Rao, T. N.; Reedijk, J.; Rijn, J.; van Verschoor, G. C. *J. Chem. Soc., Dalton Trans.* **1984**, 1349.

(33) Kühl, O. *Phosphorus-31 NMR Spectroscopy: A Concise Introduction for the Synthetic Organic and Organometallic Chemist*; Springer-Verlag: Berlin, 2008.

(34) (a) Wolf, R. *Pure Appl. Chem.* **1980**, *52*, 1141. (b) Burgada, R.; Setton, R. In *The Chemistry of Organophosphorus Compounds*; Hartley, F., Ed.; Wiley: Chichester, U.K., 1994; Vol. 3, p 185.

(35) Akiba, K. *Chemistry of Hypervalent Compounds*; Wiley-VCH: New York, 1998.

(36) Mukhlall, J. A.; Hersh, W. H. *Inorg. Chim. Acta* **2011**, *369*, 62.

(37) Arduengo, A. J. *Pure Appl. Chem.* **1987**, *59*, 1053.

(38) Couzijn, E. P. A.; Slootweg, J. C.; Ehlers, A. W.; Lammertsma, K. *J. Am. Chem. Soc.* **2010**, *132*, 18127.

(39) (a) Reed, A. E.; Schleyer, P. v. R. *J. Am. Chem. Soc.* **1990**, *112*, 1434. (b) Matsukawa, S.; Kojima, S.; Kajiyama, K.; Yamamoto, Y.; Akiba, K.-Y.; Re, S.; Nagase, S. *J. Am. Chem. Soc.* **2002**, *124*, 13154.

(40) Weinhold, F.; Landis, C. R. *Valency and Bonding: A Natural Bond Orbital Donor-Acceptor Perspective*; Cambridge University Press: Cambridge, U.K., New York, 2005; pp 275−305.
(41) Holmes, R. R.; Deiters, J. A. *J. Am. Chem. Soc.* **1977**, *99*, 3318.
(42) Comba, P.; Schiek, W. *Coord. Chem. Rev.* **2003**, *238*−*239*, 21 and references therein.
(43) (a) Murillo, A.; Chiquete, L. M.; Joseph-Nathan, P.; Contreras, R. *Phosphorus, Sulfur Silicon Relat. Elem.* **1990**, *53*, 87. (b) Camacho-Camacho, C.; Martinez-Martinez, F. J.; Rosales-Hoz, M. J.; Contreras, R. *Phosphorus, Sulfur Silicon Relat. Elem.* **1994**, *91*, 189.
(44) Khasnis, D. V.; Burton, J. M.; McNeil, J. D.; Santini, C. J.; Zhang, H.; Lattman, M. *Inorg. Chem.* **1994**, *33*, 2657.
(45) Ross, M. R.; Martin, J. C. *J. Am. Chem. Soc.* **1981**, *103*, 1234.
(46) Milbrath, D. S.; Verkade, J. G. *J. Am. Chem. Soc.* **1977**, *99*, 6607.
(47) (a) Kobayashi, J.; Goto, K.; Kawashima, T. *J. Am. Chem. Soc.* **2001**, *123*, 3387. (b) Kobayashi, J.; Kawashima, T. *C. R. Chim.* **2010**, *13*, 1249.
(48) Myers, T. W.; Berben, L. A. *J. Am. Chem. Soc.* **2013**, *135*, 9988.
(49) (a) Jana, A.; Objartel, I.; Roesky, H. W.; Stalke, D. *Inorg. Chem.* **2009**, *48*, 798. (b) Meltzer, A.; Inoue, S.; Präsang, C.; Driess, M. *J. Am. Chem. Soc.* **2010**, *132*, 3038. (c) Wang, W.; Inoue, S.; Yao, S.; Driess, M. *Organometallics* **2011**, *30*, 6490.
(50) (a) Nifantiev, E. E.; Grachev, M. K.; Burmistrov, S. Y. *Chem. Rev.* **2000**, *100*, 3755. (b) Pudovik, A. N.; Evstafev, G. I. *Dokl. Akad. Nauk SSSR* **1968**, *183*, 842.
(51) Hudson, R. F.; Brown, C. *Acc. Chem. Res.* **1972**, *5*, 204.
(52) Moerdyk, J. P.; Blake, G. A.; Chase, D. T.; Bielawski, C. W. *J. Am. Chem. Soc.* **2013**, *135*, 18798.
(53) Reich, H. J. *J. Chem. Educ.: Software* **1996**, *3D*, 2.
(54) Frisch, M. J.; Trucks, G. W.; Schlegel, H. B.; Scuseria, G. E.; Robb, M. A.; Cheeseman, J. R.; Scalmani, G.; Barone, V.; Mennucci, B.; Petersson, G. A.; Nakatsuji, H.; Caricato, M.; Li, X.; Hratchian, H. P.; Izmaylov, A. F.; Bloino, J.; Zheng, G.; Sonnenberg, J. L.; Hada, M.; Ehara, M.; Toyota, K.; Fukuda, R.; Hasegawa, J.; Ishida, M.; Nakajima, T.; Honda, Y.; Kitao, O.; Nakai, H.; Vreven, T.; Montgomery, J. A., Jr.; Peralta, J. E.; Ogliaro, F.; Bearpark, M.; Heyd, J. J.; Brothers, E.; Kudin, K. N.; Staroverov, V. N.; Kobayashi, R.; Normand, J.; Raghavachari, K.; Rendell, A.; Burant, J. C.; Iyengar, S. S.; Tomasi, J.; Cossi, M.; Rega, N.; Millam, M. J.; Klene, M.; Knox, J. E.; Cross, J. B.; Bakken, V.; Adamo, C.; Jaramillo, J.; Gomperts, R.; Stratmann, R. E.; Yazyev, O.; Austin, A. J.; Cammi, R.; Pomelli, C.; Ochterski, J. W.; Martin, R. L.; Morokuma, K.; Zakrzewski, V. G.; Voth, G. A.; Salvador, P.; Dannenberg, J. J.; Dapprich, S.; Daniels, A. D.; Farkas, Ö.; Foresman, J. B.; Ortiz, J. V.; Cioslowski, J.; Fox, D. J. *Gaussian 09*, revision B.01; Gaussian, Inc.: Wallingford, CT, 2009.
(55) (a) Zhao, Y.; Truhlar, D. G. *Theor. Chem. Acc.* **2008**, *120*, 215. (b) Zhao, Y.; Truhlar, D. G. *Acc. Chem. Res.* **2008**, *41*, 157.